PREPARATION, STRUCTURE AND ELECTRICAL PROPERTIES OF $\mathbf{Li_{1+4x}Ti_{2-x}Nb_yP_{3-y}O_{12}}$ ($\mathbf{x = 0.1, 0.2, 0.3}$; $\mathbf{y = 0, 0.1, 0.2, 0.3}$) CERAMICS

V. Venckutė [a], J. Banytė [a], V. Kazlauskienė [b], J. Miškinis [b], T. Šalkus [a], A. Kežionis [a], E. Kazakevičius [a], A. Dindune [c], Z. Kanepe [c], J. Ronis [c], and A.F. Orliukas [a]

[a] *Faculty of Physics, Vilnius University, Saulėtekio 9, LT-10222, Vilnius, Lithuania*
E-mail: vilma.venckute@stud.vu.lt
[b] *Institute of Applied Research, Vilnius University, Saulėtekio 9, LT-10222 Vilnius, Lithuania*
[c] *Institute of Inorganic Chemistry, Riga Technical University, Miera iela 34, LV-2169 Salaspils, Latvia*

The solid electrolyte compounds of $Li_{1+4x}Ti_{2-x}Nb_yP_{3-y}O_{12}$ ($x = 0.1, 0.2, 0.3$; $y = 0, 0.1, 0.2, 0.3$) were synthesized by a solid state reaction and studied by X-ray diffraction from the powder. At room temperature all of the compounds display the hexagonal symmetry (space group R$\bar{3}$c) with six formula units in the unit cell. The values of the binding, splitting energies and amounts of elements of Ti 2p, Nb 3d, P 2p, O 1s, and Li 1s core level of the ceramics' surfaces have been determined by XPS. Impedance spectroscopy of the ceramics has been performed in the frequency range of 10–$3{\cdot}10^9$ Hz in the temperature interval 300–600 K. The insertion of niobium into the host compound $Li_{1.4}Ti_{1.9}P_3O_{12}$ leads to the changes of the value of ionic conductivity and its activation energy for the new ceramics.

Keywords: ceramics, XRD, XPS, ionic conductivity

PACS: 66.10.Ed, 61.43.Gt, 52.25.Mq

1. Introduction

The development of fast lithium conductors is attracting much attention because of their applications in high-energy Li-ion batteries [1, 2] and electrochemical sensors [3]. It is known that $LiTi_2P_3O_{12}$ compound with the NASICON-type structure is a pure ionic conductor [4, 5]. Its bulk ionic conductivity at room temperature was found to be $\sigma_b = 2{\cdot}10^4$ S/m [4, 6]. It has been used as a host compound for investigation of lithium ion transport peculiarities and a series of new Li-ion conductors have been obtained by different ion substitution [4, 5]. The system $Li_{1+x}M_xTi_{2-x}(PO_4)_3$ (where M = Al, Sc, Y, Fe, Cr) seems to be the most suitable for Li^+ ionic transport in the framework [4, 7]. Conductivity increases rapidly when Ti^{4+} is partially substituted by $M^{III} + Li^+$ ions in the abovementioned system [4] or P^{5+} is substituted by Si^{4+} [8]. High ionic conductivity of abovementioned NASICON-type structure solid electrolyte compounds stimulates further investigation and makes the materials promising for applications in the functional elements of solid state ionics. The aim of this paper is to investigate the influence of partial substitution of P^{5+} by Nb^{5+} on the structure parameters, surface and electric properties of the $Li_{1+4x}Ti_{2-x}Nb_yP_{3-y}O_{12}$ (where $x = 0.1, 0.2, 0.3$; $y = 0, 0.1, 0.2, 0.3$) ceramics. In this study, we report the conditions of powder preparation, the results of powder X-ray diffraction (XRD), X-ray photoelectron spectroscopy (XPS), and electrical properties of the ceramics in the frequency range from 10 to $3{\cdot}10^9$ Hz in the temperature range from 300 to 600 K.

2. Experiment

Conventional solid-state reaction method was employed to prepare $Li_{1+4x}Ti_{2-x}Nb_yP_{3-y}O_{12}$ (where $x = 0.1, 0.2, 0.3$; $y = 0, 0.1, 0.2, 0.3$) compounds. Appropriate mixed and milled stoichiometric amounts of Li_2CO_3 (purity 99.999%), TiO_2, Nb_2O_5, and $NH_4H_2PO_4$ (extra pure) were heated at temperature $T = 723$ K for 20 h. After heating the mixture was placed in ethyl alcohol and milled in a planetary mill for 12–24 h. The obtained powders were heated at temperature 973–1073 K for 3–8 h, then at 1173 K for 3 h, and at 1273 K for 3 h. The last step of heat

treatment for compound which contained Nb ($y = 0.1$) was at 1473 K for 2 h. After each heating the mixture was placed in ethyl alcohol and milled in a planetary mill. Finally, the obtained powders were dried at 393 K temperature for 24 h.

The structure parameters were obtained using Bruker D8 Advance equipment at room temperature from the X-ray powder diffraction patterns in the region $2\Theta = 10$–80 degree, step 0.02 degree, time per step 1 s, Cu $K_{\alpha 1}$ radiation (40 kV, 40 mA). The lattice parameters were deduced by fitting the XRD patterns with software TOPAS.

The ceramic samples were used for XPS and impedance measurements. The powder was uniaxially cold pressed at 300 MPa. The sintering of the samples was conducted in air. The sintering temperature of ceramics $Li_{1+4x}Ti_{2-x}P_3O_{12}$ ($x = 0.1$) and $Li_{1+4x}Ti_{2-x}Nb_yP_{3-y}O_{12}$ ($x = 0.2, 0.3$; $y = 0.1, 0.2, 0.3$) was 1343 and 1223 K respectively. The sintering duration of the ceramics was 1 h. Chemical bonding states of the constituent elements of the surfaces of ceramics were examined by X-ray photoelectron spectroscopy. XPS were recorded by LAS-3000 (ISA-Riber) surface analysis equipment. The instrument was equipped with double-pass cylindrical mirror analyzer MAC2. The XPS were obtained by using Mg K_{α} ($h\nu = 1253.6$ eV) radiation at an average of 10 scans with step size of 0.05 eV. Before the measurement the samples were kept in a preparation chamber (residual pressure $1.6 \cdot 10^{-6}$ Pa) of the experimental setup for one day. The residual pressure in the analyzer chamber was $1.3 \cdot 10^{-8}$ Pa. In order to extract the core-level shifts and relative intensities of these components, a curve-fitting procedure was utilized. The fitting of the core-level data was performed using a nonlinear fitting procedure (software XPSPEAK 41).

Platinum electrodes were prepared on sintered cylindrical samples by conductive Pt paste (GVENT Electronic Materials LTD) fired at 1073 K. For the measurements of electrical impedance in the frequency range 10–$2 \cdot 10^6$ Hz vector voltmeter-amperemeter method was used. The network with the sample was affected by the narrow spectra radio pulse. Voltage and current of this network were measured by two channel computer oscilloscope TiePie Handyscope HS3. For ac current measurement a special current–voltage converter, allowing accurate vector current converting, was used. The accurate complex impedance ($\tilde{Z} = Z' - iZ''$) and complex dielectric permittivity of the samples were computed by computer from amplitude and phase measurements of the signals. The measurements in the frequency range $3 \cdot 10^5$–$3 \cdot 10^9$ Hz were performed by Agilent Network Analyzer E5062A connected to a coaxial line, the part of inner conductor of which was replaced by the sample. The impedance of the sample was calculated from transmission and reflection parameters of such network. The temperature measurements of the ceramics in the low and high frequency ranges were performed in the range of 300–600 K by Digital Thermometer TMD90A. The temperature was controlled by a computer connected to dc power supply Mastech HY 30005.

3. Results and discussion

Figure 1 shows powder X-ray diffraction patterns of $Li_{1+4x}Ti_{2-x}Nb_yP_{3-y}O_{12}$ ($x = 0.1, 0.2, 0.3$; $y = 0, 0.1, 0.2, 0.3$) compounds. The results of XRD data analysis have shown that $LiTiPO_5$ impurities are present in compounds with $y = 0, 0.1, 0.2, 0.3$ and they are marked with asterisks in Fig. 1. In compounds with $y = 0, 0.1, 0.2,$ and 0.3 the amounts of impurities were found to be 2, 3, 8, and 17% respectively. The investigated compounds display the hexagonal symmetry (space group $R\bar{3}c$). The lattice parameters, unit cell volume (V), theoretical density (d_{X-ray}), and formula units in the lattice (Z) of the investigated compounds are presented in Table 1. The relative density of the ceramics was found to be 94% of the theoretical density.

XP spectra of surface of $Li_{1+4x}Ti_{2-x}Nb_yP_{3-y}O_{12}$ ($x = 0.1, 0.2, 0.3$; $y = 0, 0.1, 0.2, 0.3$) ceramics are shown in Fig. 2(a–e). To exclude any effects on the values of binding energies due to charging of the sample during the XPS analysis, all data were corrected by a linear shift such that the peak maximum of the C 1s binding energy of adventitious carbon corresponded to 284.6 eV. Ti 2p, P 2p, Nb 3d, O 1s, and Li 1s core level XP spectra were fitted. Ti 2p spectrum is shown in Fig. 2(a). The spectrum shows spin–orbit doublet of Ti $2p_{3/2}$ and Ti $2p_{1/2}$ as in [9]. The spin–orbit doublets assembled two low and high binding energy peaks. The lower energy peaks of Ti $2p_{3/2}$ spectra are in the range from 458.5 to 459.1 eV. The higher binding energy peaks of Ti $2p_{1/2}$ spectra are in range from 459.7 to 460.1 eV. The binding splitting energies of $2p_{3/2}$ and $2p_{1/2}$ spectra depend on stoichiometric parameters x and y of the investigated compounds. The splitting is in the range between 5.8 and 6.1 eV. The authors [9] reported that binding energy splitting between $2p_{3/2}$ and $2p_{1/2}$ in $LiM_{0.05}Mn_{1.95}O_4$ (M = Ni, Fe, and Ti) solid electrolytes is 5.4 eV. Ti 2p spectrum has been deconvoluted into two spin–orbit doublets. The $2p_{3/2}$ peaks

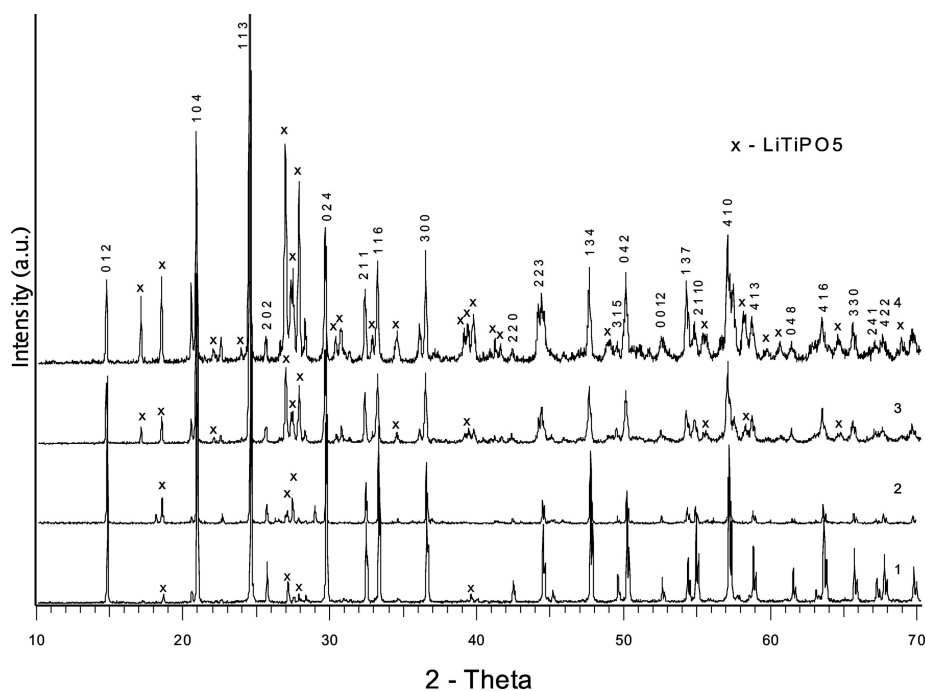Fig. 1. The powder X-ray diffraction patterns of $Li_{1+4x}Ti_{2-x}Nb_yP_{3-y}O_{12}$ compounds: *1* ($x = 0.1$, $y = 0$); *2* ($x = 0.1$, $y = 0.1$); *3* ($x = 0.2$, $y = 0.2$); *4* ($x = 0.3$, $y = 0.3$).

Table 1. Summary of X-ray diffraction results for $Li_{1+4x}Ti_{2-x}Nb_yP_{3-y}O_{12}$ compounds at room temperature.

Compound	a (Å)	c (Å)	V (Å^3)	$d_{X\text{-ray}}$ (g cm^{-3})	Z
$Li_{1.4}Ti_{1.9}P_3O_{12}$	8.5137(2)	20.8587(5)	1309.36	2.93	6
$Li_{1.4}Ti_{1.9}Nb_{0.1}P_{2.9}O_{12}$	8.5267(23)	20.8608(53)	1313.49	2.97	6
$Li_{1.8}Ti_{1.8}Nb_{0.2}P_{2.8}O_{12}$	8.5257(6)	20.8975(35)	1315.49	3.00	6
$Li_{2.2}Ti_{1.7}Nb_{0.3}P_{2.7}O_{12}$	8.5242(7)	20.8976(27)	1315.04	3.03	6

at lower binding energy are associated with a lower oxidation state (Ti^{3+}). The peaks at higher $2p_{3/2}$ binding energy are associated with the Ti^{4+} state [10]. The ratio of Ti^{4+} and Ti^{3+} was determined by fitting and estimating the area of each doublet and it corresponds to different amounts of Ti^{4+} and Ti^{3+} states. The different amount of Ti^{4+} and Ti^{3+} was found in Li conducting solid electrolytes such as $LiM_{0.05}Mn_{1.95}O_4$ (M = Ni, Fe, and Ti) [9] or Li_2O–Al_2O_3–(TiO_2 or GeO_2)–P_2O_5 glass–ceramics [10]. The results of XRD investigation have shown that in the compounds with stoichiometric parameter $y = 0, 0.1, 0.2, 0.3$ some lines related to $LiTiPO_5$ exist. The values of the binding and splitting energies and amounts of Ti^{4+} and Ti^{3+} states in atomic % and the chi-square parameter are presented in Table 2. The deconvolution of the P 2p XP spectra of $Li_{1+4x}Ti_{2-x}Nb_yP_{3-y}O_{12}$ ($x = 0.1, 0.2, 0.3$; $y = 0, 0.1, 0.2, 0.3$) ceramics into two peaks is shown in Fig. 2(b). The deconvolution of the P 2p core level XPS can be associated with different amounts of P^{5+}

and P^{3+} states in the investigated ceramics. The P^{5+} and P^{3+} states in the ceramics can be associated with group PO_4^{3-} and group PO_3^- respectively. The values of the binding energies and amounts of P^{5+} and P^{3+} states in atomic % and the chi-square parameter are presented in Table 2. Figure 2(c) shows the fitting pattern of O 1s XP spectra of $Li_{1+4x}Ti_{2-x}Nb_yP_{3-y}O_{12}$ (where $x = 0.1, 0.2, 0.3$; $y = 0, 0.1, 0.2, 0.3$) ceramic surfaces. It can be seen that the O 1s core level XP spectra has been deconvoluted into four peaks. For O 1s, some peaks with binding energies in the range from 529.8 to 531.1 eV are attributed to the lattice oxygen at the normal sites of the NASICON structure and other O 1s are assigned to the chemisorbed oxygen in the forms O^{2-}, O_2^-, and in hydroxyl environment (OH) as in $La_{0.6}Sr_{0.4}Co_{1-y}Fe_xO_3$ ceramics [11]. The fitting pattern of O 1s core level XP spectrum is summarized in Table 2. Figure 2(d) shows Nb 3d spectra of investigated ceramics. The spectrum shows spin–orbit doublet of Nb $3d_{5/2}$ and Nb $3d_{3/2}$ as in $LiNbO_3$ [12] or potassium lithium niobate [13] crystals. The
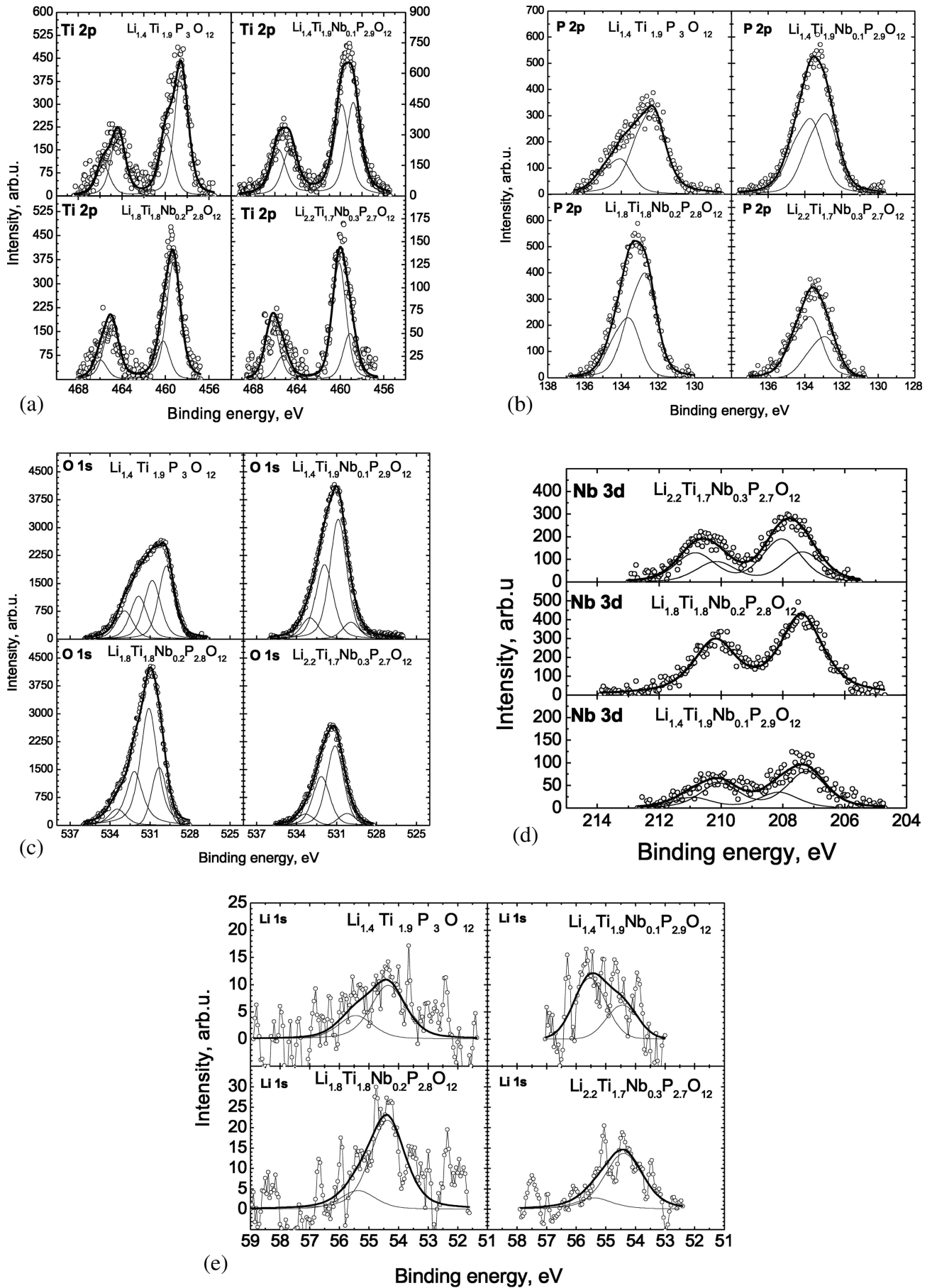
Fig. 2. (a) Ti 2p, (b) P 2p, (c) Nb 3d, (d) O 1s, and (e) Li 1s core level XP spectra.

Table 2. The binding, splitting energies of XPS spectra, amounts of the elements, and chi-square values of $Li_{1+4x}Ti_{2-x}Nb_yP_{3-y}O_{12}$ ($x = 0.1, 0.2, 0.3$; $y = 0, 0.1, 0.2, 0.3$) compounds.

Compound		Binding energy, eV	Splitting energy, eV	Amount, at. %	χ
$Li_{1.4}Ti_{1.9}P_3O_{12}$	O 1s	529.8		34.3	2.19
		530.8		29.7	
		531.9		21.7	
		532.9		14.3	
	P 2p$_{3/2}$	132.2	0.95	72.1	1.46
		133.9	0.95	27.9	
	Ti 2p$_{3/2}$	458.5	5.8	67.2	1.1
		459.7	5.8	32.8	
	Li 1s	54.6		71.7	0.34
		55.7		28.3	
$Li_{1.4}Ti_{1.9}Nb_{0.1}P_{2.9}O_{12}$	O 1s	529.9		7.2	1.7
		530.9		50.9	
		532.0		32.7	
		533.0		9.2	
	P 2p$_{3/2}$	132.8	1.0	50.4	1.04
		133.6	1.0	49.6	
	Li 1s	54.5		36.1	0.35
		55.5		63.9	
	Nb 3d$_{5/2}$	207.2	2.8	69.9	0.47
		208.1	2.8	30.1	
	Ti 2p$_{3/2}$	458.8	5.8	49.9	1.1
		459.9	5.8	50.1	
$Li_{1.8}Ti_{1.8}Nb_{0.2}P_{2.8}O_{12}$	O 1s	530.3		17.2	3.7
		531.1		50.6	
		532.2		25.3	
		533.5		6.9	
	P 2p$_{3/2}$	132.6	0.95	64.9	1.17
		133.5	0.95	35.1	
	Li 1s	54.4		85	0.39
		55.4		15	
	Nb 3d$_{5/2}$	207.4	2.8	100	1.3
	Ti 2p$_{3/2}$	459.3	5.7	77.0	0.89
		460.2	5.8	23.0	
$Li_{2.2}Ti_{1.7}Nb_{0.3}P_{2.7}O_{12}$	O 1s	530.2		7.0	1.6
		531.1		52.8	
		532.2		32.6	
		533.3		7.6	
	P 2p$_{3/2}$	132.8	1.0	36.6	1.4
		133.6	1.0	63.4	
	Li 1s	54.4		81.7	0.1
		55.4		18.3	
	Nb 3d$_{5/2}$	207.4	2.8	41.3	1.03
		208.0	2.8	58.7	
	Ti 2p$_{3/2}$	459.1	6.1	29.3	0.69
		460.1	6.1	70.7	

deconvolution of the Nb 3d core level XP spectrum can be associated with different amounts of Nb^{5+} and Nb^{4+} [12] or lower (Nb^{3+}) valence states in the investigated ceramics. The amount of different Nb valence states, binding and splitting energies of Nb $3d_{5/2}$ and Nb $3d_{3/2}$ core level XP spectra are presented in Table 2. Li 1s core level XP spectra of the investigated ceramics are shown in Fig. 2(e). Li 1s signal is of very low intensity and the fitting of the patterns is very complicated. Li 1s core level XP spectra of all $Li_{1+4x}Ti_{2-x}Nb_yP_{3-y}O_{12}$ compounds have been deconvoluted into two peaks. The binding energies of Li 1s spectra depend on stoichiometric parameters x and y of the investigated compounds. For the compound with $y = 0$ one peak is at lower binding energy (54.6 eV), the other peak is at higher binding energy (55.7 eV). The increase of the stoichiometric parameter y of investigated compounds leads to the decrease of binding energies of Li 1s core level XP spectra. In the ceramics with $y = 0.2, 0.3$ the two peaks at lower binding energy are centred at the same values (54.4 eV) and peaks at higher binding energies are centred at 55.4 eV (Table 2). The values of the binding energy of Li 1s core level XP spectra well correlate with results reported in [14, 15]. It is reported that the Li 1s core level XP spectrum peak is at the binding energy of around 55.8 eV [14]. For the $Li_{0.8}CoO_4$ composition a single Li 1s peak has been observed at 55.4 eV, but for Li rich compositions such as $LiCoO_4$ and $Li_{1.2}CoO_4$ an intense peak is at 55.4 eV and a shoulder peak around 55.05 eV has also been observed [15]. The different binding energies of Li 1s spectra can be associated with two different positions of Li ions in the lattice of investigated compounds. The results of the NMR study of $LiTi_{2-x}Zr_x(PO_4)_3$ composition have shown that Li ions occupy two different positions in the lattice, too [6].

Three relaxation dispersions have been found in complex conductivity and impedance spectra of the studied ceramics. The one in the high frequency region was attributed to Li^+ ion relaxation in the bulk whereas the intermediate frequency range dispersion was caused by ion blocking effect at grain boundaries of the ceramics. The low frequency region of the dispersion is associated with electrode processes. Frequency dependences of the real part of complex conductivity of $Li_{1+4x}Ti_{2-x}Nb_yP_{3-y}O_{12}$ ($x = 0.1, 0.2, 0.3; y = 0, 0.1, 0.2, 0.3$) ceramics measured at temperature $T = 530$ K are shown in Fig. 3. The dispersion regions shift to higher frequencies while temperature is increased. Bulk (σ_b) and to-
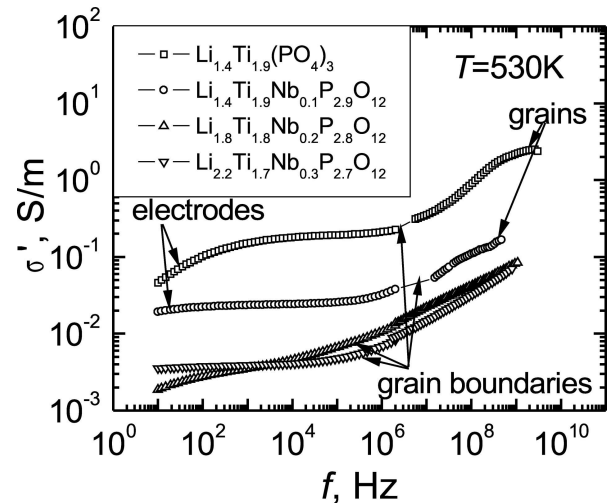

Fig. 3. Frequency dependences of the real part of conductivity of $Li_{1+4x}Ti_{2-x}Nb_yP_{3-y}O_{12}$ ($x = 0.1$ 0.2, 0.3; $y = 0, 0.1, 0.2, 0.3$) ceramics.
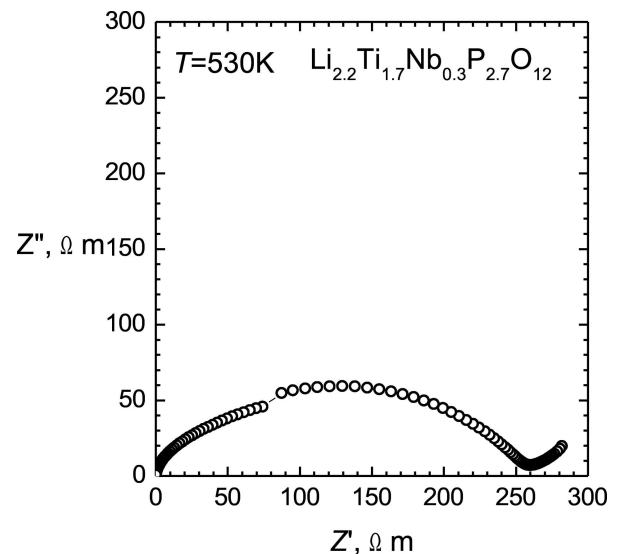

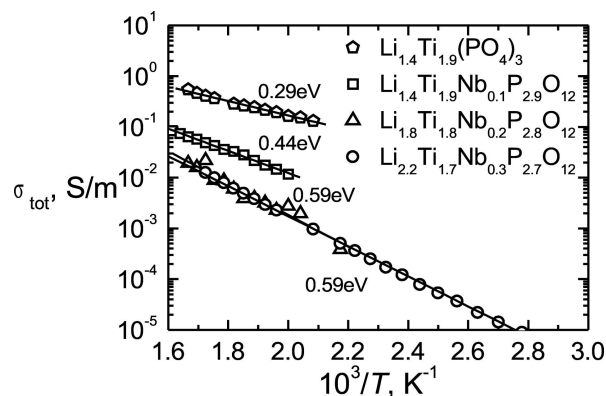Fig. 4. Characteristic impedance complex plane plot of ceramics $Li_{2.2}Ti_{1.7}Nb_{0.3}P_{2.7}O_{12}$.

tal (σ_{tot}) conductivities were derived from impedance complex plane $Z''(Z')$ and conductivity complex plane $\sigma''(\sigma')$ plots. The characteristic $Z''(Z')$ and $\sigma''(\sigma')$ plots of $Li_{2.2}Ti_{1.7}Nb_{0.3}P_{2.7}O_{12}$ ceramics at temperature $T = 530$ K can be seen in Figs. 4 and 5 respectively. Temperature dependences of σ_{tot} and σ_b of $Li_{1+4x}Ti_{2-x}Nb_yP_{3-y}O_{12}$ ($x = 0.1, 0.2, 0.3; y = 0, 0.1, 0.2, 0.3$) ceramics are shown in Figs. 6 and 7 respectively. σ_b and σ_{tot} of investigated ceramics change according to Arrhenius law in the studied temperature range. The values of σ_b and σ_{tot} as well as their activation energies ΔE_b and ΔE_{tot} are summarized in Table 3. The comparing of results of the XRD and conductivity investigations has shown that the increases

Table 3. σ_b, σ_{tot}, and their activation energies of $Li_{1+4x}Ti_{2-x}Nb_yP_{3-y}O_{12}$ ceramics at temperature $T = 530$ K.

Compounds	σ_b, S m^{-1}	ΔE_b, eV	σ_{tot}, S m^{-1}	ΔE_{tot}, eV
$Li_{1.4}Ti_{1.9}P_3O_{12}$	2.07	0.18	0.244	0.29
$Li_{1.4}Ti_{1.9}Nb_{0.1}P_{2.9}O_{12}$	0.22	0.38	0.022	0.44
$Li_{1.8}Ti_{1.8}Nb_{0.2}P_{2.8}O_{12}$	0.05	0.4	0.004	0.59
$Li_{2.2}Ti_{1.7}Nb_{0.3}P_{2.7}O_{12}$	0.04	0.43	0.0038	0.59
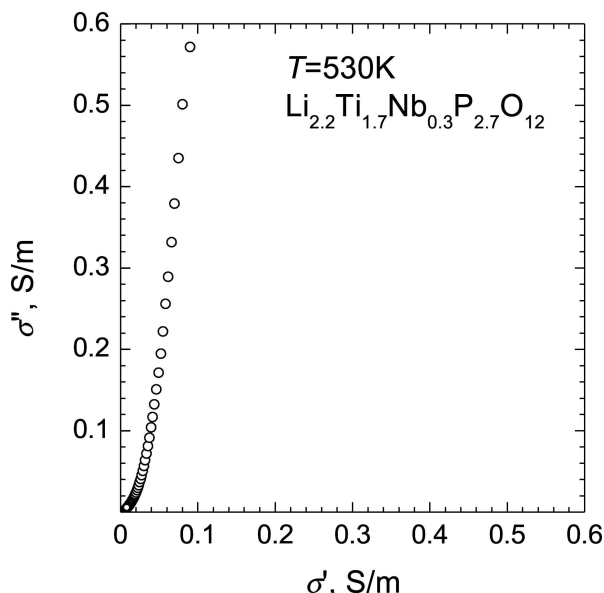
Fig. 5. Characteristic conductivity complex plane plot of ceramics $Li_{2.2}Ti_{1.7}Nb_{0.3}P_{2.7}O_{12}$.

Fig. 6. Temperature dependences of total conductivities of ceramics $Li_{1+4x}Ti_{2-x}Nb_yP_{3-y}O_{12}$.
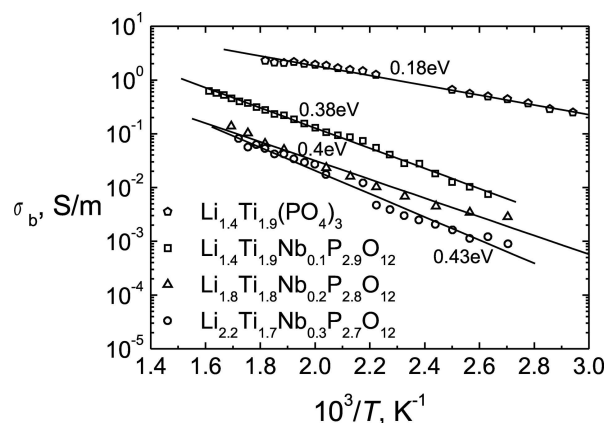
Fig. 7. Temperature dependences of bulk conductivities of ceramics $Li_{1+4x}Ti_{2-x}Nb_yP_{3-y}O_{12}$.

of amounts of the impurities $LiTiPO_5$ lead to the decrease of total and bulk conductivities and increase their activation energies. According to [16] the compound $LiTiPO_5$ exhibits a very low electrical conductivity ($(5–10)\cdot10^{-4}$ S/m at 673 K, its activation energy $\Delta E \approx 1$ eV). On the other hand, the values of conductivities and their activation energies depend on the ratios Li/Ti and Li/Nb in the investigated compounds. The results of the XPS investigation showed that the ratio Li/Nb in the compounds with stoichiometric parameter $y = 0.1$, 0.2, and 0.3 was 14, 9, and 7 respectively. The ratio Li/Ti in the compounds with stoichiometric parameter $y = 0$, 0.1, 0.2, and 0.3 was found to be 0.73, 0.7, 1, and 1.29 respectively. The decrease of Li/Nb or the increase of Li/Ti ratios in the investigated compounds caused a decrease of the values of bulk conductivity and a decrease of their activation energy. The temperature dependences of real part of dielectric permittivity (ε') and losses ($\tan\delta$) measured at frequency 1 GHz are presented in Figs. 8 and 9 respectively. At room temperature the value of ε' of $Li_{1.4}Ti_{1.9}P_3O_{12}$ ceramic was found to be 12 and decreased with the increase of stoichiometric parameters x, y and amount

of impurities in the ceramics, too (at room temperature the value of ε' of compound with $y = 0.3$ was found to be 7). The increase of the values of ε' of the investigated compounds with temperature can be caused by contribution of the migration polarization of lithium ions, vibration of lattice, and electronic polarization. The increase of $\tan\delta$ with temperature is related to the contribution of conductivity in the investigated temperature region.

4. Conclusions

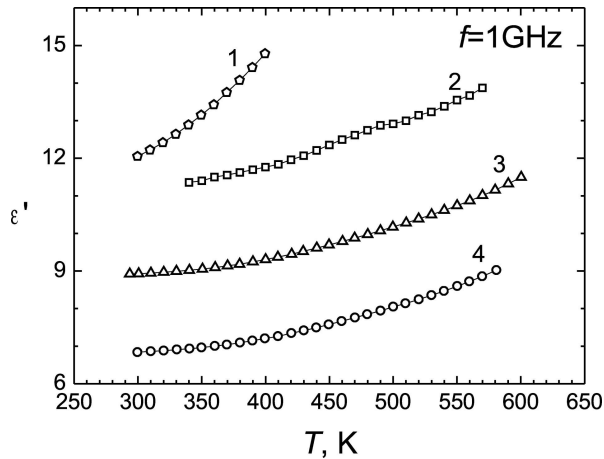The powder of $Li_{1+4x}Ti_{2-x}Nb_yP_{3-y}O_{12}$ ($x = 0.1$, 0.2, 0.3; $y = 0$, 0.1, 0.2, 0.3) has been prepared by solid

Fig. 8. Temperature dependences of dielectric permittivity of ceramics $Li_{1+4x}Ti_{2-x}Nb_yP_{3-y}O_{12}$: *1* ($x = 0.1$, $y = 0$); *2* ($x = 0.1$, $y = 0.1$); *3* ($x = 0.2$, $y = 0.2$); *4* ($x = 0.3$, $y = 0.3$).
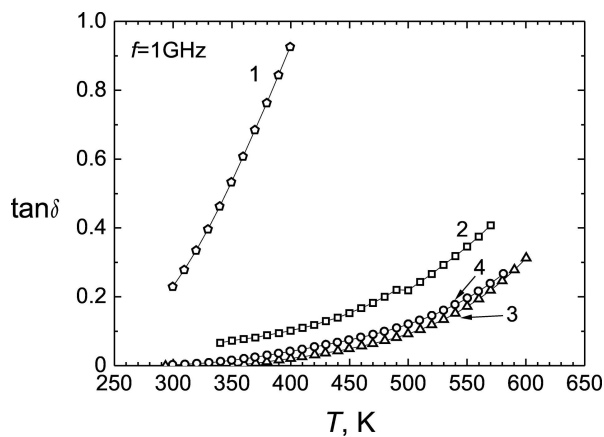
Fig. 9.   Temperature dependences of $\tan\delta$ of ceramics $Li_{1+4x}Ti_{2-x}Nb_yP_{3-y}O_{12}$: *1* ($x = 0.1$, $y = 0$); *2* ($x = 0.1$, $y = 0.1$); *3* ($x = 0.2$, $y = 0.2$); *4* ($x = 0.3$, $y = 0.3$).

state reaction and ceramics have been sintered. The results of XRD have shown that investigated compounds belong to hexagonal symmetry (space group R$\bar{3}$c). In all the compounds the impurities LiTiPO$_5$ are present. Ti 2p, P 2p, Nb 3d, O 1s, and Li 1s core level XP spectra were fitted. The results of the XPS investigation suggest that Ti ions are in Ti^{3+} and Ti^{4+} oxidation states. It was ascertained that there are four different kinds of oxygen on the ceramic surface, including lattice oxygen, chemisorbed oxygen in the forms O^{2-}, O$_2^-$, and oxygen in hydroxyl environment (OH). The deconvolution of the P 2p core level XP spectrum can be associated with different amounts of P^{5+} and P^{3+} states in the investigated ceramics. The P^{5+} and P^{3+} states in the ceramics can be associated with group PO$_4^{3-}$ and group PO$_3^-$ respectively. The deconvolution of the Nb 3d core level XP spectrum can be associated with dif-

ferent amounts of Nb^{5+} and Nb^{4+} or lower (Nb^{3+}) valence states in the investigated ceramics.

Impedance spectroscopy study of the ceramics in the frequency range of 10–10^9 Hz in the temperature range from 300 to 600 K has revealed that an increase of the stoichiometric parameters x, y and amount of impurities LiTiPO$_5$ or a decrease of the Li/Nb, or an increase of Li/Ti ratios in the investigated Li$_{1+4x}$Ti$_{2-x}$Nb$_y$P$_{3-y}$O$_{12}$ compounds lead to the decrease of total and bulk conductivities and are increasing their activation energies. At room temperature the value of ε' of Li$_{1.4}$Ti$_{1.9}$P$_3$O$_{12}$ ceramic was found to be 12 and it decreases with the increase of stoichiometric parameters x and y of Li$_{1+4x}$Ti$_{2-x}$Nb$_y$P$_{3-y}$O$_{12}$ ceramics.

Acknowledgement

References

[1] V. Thangadurai, J. Schwenzel, and W. Weppner, Tailoring ceramics for specific applications: a case study of the development of all-solid-state lithium batteries, Ionics **11**, 11–23 (2005).

[2] M. Broussely, J.P. Planchot, G. Rigobert, D. Vireu, and G. Sarre, Lithium-ion batteries for electric vehicles: performances of 100 Ah cells, J. Power Sources **68**, 8–12 (1997).

[3] F. Salam, P. Birke, and W. Weppner, Solid-state CO$_2$ sensor with Li$_2$CO$_3$–MgO electrolyte and LiMn$_2$O$_4$ as solid reference electrode, Electrochem. Solid-State Lett. **2**(4), 201–204 (1999).

[4] H. Aono, E. Sugimoto, Y. Sadaoka, N. Imanaka, and G. Adachi, Ionic conductivity of solid electrolytes based on lithium titanium phosphate, J. Electrochem. Soc. **137**(4), 1023–1027 (1990).

[5] M.A. Subramanian, R. Subramanian, and A. Clearfield, Lithium ion conductors in the system AB(IV)$_2$(PO$_4$)$_3$ (B = Ti, Zr and Hf), Solid State Ionics **18–19**, 562–569 (1986).

[6] K. Arbi, J.M. Rojo, and J. Sanz, Lithium mobility in titanium based Nasicon Li$_{1+x}$Ti$_{2-x}$Al$_x$(PO$_4$)$_3$ and LiTi$_{2-x}$Zr$_x$(PO$_4$)$_3$ materials followed by NMR and impedance spectroscopy, J. Eur. Ceram. Soc. **27**, 4215–4218 (2007).

[7] H. Aono, E. Sugimoto, Y. Sadaoka, N. Imanaka, and G-y. Adachi, Ionic conductivity and sinterability of lithium titanium phosphate system, Solid State Ionics **40–41**, 38–42 (1990).

[8] A. Dindune, A. Kežionis, Z. Kanepe, E. Kazake-vičius, R. Sobiestianskas, and A. Orliukas, Synthesis and ionic conductivity of phosphate materials obtained in the systems Li_2O–$Sc(Ti,Al,Si)_2O_3$–P_2O_5, Phosphorus Res. Bull. **10**, 387–392 (1999).

[9] Qi-Hui Wu, Jin-Mei Xu, Quan-Chao Zhuang, and Shi-Gang Sun, X-ray photoelectron spectroscopy of $LiM_{0.05}Mn_{1.95}O_4$ (M = Ni, Fe and Ti), Solid State Ionics **177**, 1483–1488 (2006).

[10] B.V.R. Chowdari, G.V. Subba Rao, and G.Y.H. Lee, XPS and ionic conductivity studies on Li_2O–Al_2O_3–(TiO_2 or GeO_2)–P_2O_5 glass–ceramics, Solid State Ionics **136–137**, 1067–1075 (2000).

[11] Qing Xu, Duan-ping Huang, Wen Chen, Hao Wang, Bi-tao Wang, and Run-zhang Yuan, X-ray photoelectron spectroscopy investigation on chemical states of oxygen on surfaces of mixed electronic-ionic conducting $La_{0.6}Sr_{0.4}Co_{1-y}Fe_yO_3$ ceramics, Appl. Surf. Sci. **228**, 110–114 (2004).

[12] R.J. Iwanowski, M. Heinonen, I. Pracka, J. Raczyńska, K. Fronc, and J.W. Sobczak, Application of in situ surface scraping for extracting bulk component of XPS signal – example of $LiNbO_3$ and GaSb, J. Alloys Compounds **286**, 162–166 (1999).

[13] Byeong-Eog Jun, Chung-Sik Kim, Hyung-Kook Kim, Jung-Nam Kim, and Yoon-Hwae Hwang, Ar-ion etching effects on the XPS spectra of the ferroelectric potassium lithium niobate crystal, J. Korean Phys. Soc. **46**, 100–103 (2005).

[14] J. Swiatowska-Mrowiecka, S. de Diesbach, V. Maurice, S. Zanna, L. Klein, E. Briand, I. Vickridge, and P. Marcus, Li-ion intercalation in thermal oxide thin films of MoO_3 as studied by XPS, RBS, and NRA, J. Phys. Chem. C **112**, 11050–11058 (2008).

[15] M.S. Bhuvaneswari, S. Selvasekarapandian, Shinobu Fujihara, and Shinnosuke Koji, Structural, XPS and impedance analysis of Li_xCoVO_4 (x = 0.8, 1.0, 1.2), Solid State Ionics **177**, 121–127 (2006).

[16] A. Robertson, J.G. Fletcher, J.M.S. Skakle, and A.R. West, Synthesis of $LiTiPO_5$ and $LiTiAsO_5$ with the α-Fe_2PO_5 structure, J. Solid State Chem. **109**, 53–59 (1994).

$Li_{1+4x}Ti_{2-x}Nb_yP_{3-y}O_{12}$ (x = 0,1; 0,2; 0,3; y = 0; 0,1; 0,2; 0,3) KERAMIKŲ GAMYBA, STRUKTŪRA IR JŲ ELEKTRINĖS SAVYBĖS

V. Venckutė [a], J. Banytė [a], V. Kazlauskienė [b], J. Miškinis [b], T. Šalkus [a], A. Kežionis [a], E. Kazakevičius [a], A. Dindune [c], Z. Kanepe [c], J. Ronis [c], A.F. Orliukas [a]

[a] *Vilniaus universiteto Fizikos fakultetas, Vilnius, Lietuva*
[b] *Vilniaus universiteto Taikomųjų mokslų institutas, Vilnius, Lietuva*
[c] *Rygos technikos universiteto Neorganinės chemijos institutas, Ryga, Latvija*

Santrauka

$Li_{1+4x}Ti_{2-x}Nb_yP_{3-y}O_{12}$ (x = 0,1; 0,2; 0,3; y = 0; 0,1; 0,2; 0,3) junginių milteliai buvo sintezuoti kietųjų kūnų reakcijos metodu. Pagamintų keramikų tankis siekė apie 94% jų teorinio tankio. Kambario temperatūroje tirti junginiai priklauso heksagoninei singonijai (jų erdvinė grupė yra $R\bar{3}c$). Visuose junginiuose yra aptinkamos $LiTiPO_5$ priemaišos. Gauti Ti 2p, P 2p, Nb 3d, O 1s ir Li 1s Rentgeno fotoelektronų spektrai. Ti 2p Rentgeno fotoelektronų spektrų analizė rodo, kad Ti jonai tirtuose junginiuose gali būti trivalenčiai ir keturvalenčiai. O 1s spektruose dominuoja keturios smailės su skirtingomis ryšio energijomis. Tai susiję su keturiomis deguonies energinėmis būsenomis keramikų paviršiuose: gardeliniu deguonimi, chemiškai absorbuotu O^{2-} ir O_2^- būsenų deguonimi bei deguonimi hidroksilinėje (OH) jungtyje. P 2p Rentgeno fotoelektronų spektro skilimas į dvi smailes gali būti aiškinamas skirtingais fosforo katijonų P^{5+} ir P^{3+} kiekiais tirtose keramikose.

P^{5+} ir P^{3+} katijonai keramikų paviršiuose atitinkamai gali sudaryti PO_4^{3-} ir PO_3^- jungtis. Nb 3d Rentgeno fotoelektronų spektro skilimas į dvi smailes gali būti siejamas su skirtingais Nb^{5+} ir Nb^{4+} ar netgi žemesnio (Nb^{3+}) valentingumo katijonų kiekiais tirtų keramikų paviršiuose.

Elektrinės keramikų savybės buvo tirtos 10–3·10^9 Hz dažnių ir 300–600 K temperatūros intervaluose. Tyrimų rezultatai rodo, kad keramikose reiškiasi dvi relaksacinės dispersijos, kurios nusakomos jonų pernaša keramikų tarpkristalitinėse sandūrose bei kristalituose. Stechiometrijos parametrų x ir y didėjimas lemia $LiTiPO_5$ priemaišinės fazės santykinį didėjimą tirtuose junginiuose. Toks $LiTiPO_5$ kiekio didėjimas mažina dielektrinę skvarbą, bendrąjį ir kristalitinį joninius laidumus bei didina jų aktyvacijos energijas. Tirtų keramikų santykinės dielektrinės skvarbos vertės didėja kylant temperatūrai. Tokį temperatūrinį kitimą lemia migracinės, tampriosios joninės bei elektroninės poliarizacijų indėliai į tirtųjų keramikų ε' vertes.